

Increased Lifetime for Biomass and Waste to Energy Power Plant Boilers with HVOF Coatings: High Temperature Corrosion Testing Under Chlorine-Containing Molten Salt

Maria Oksa, Satu Tuurna, and Tommi Varis

(Submitted September 30, 2012; in revised form March 19, 2013)

Heat exchanger surfaces of waste to energy and biomass power plant boilers experience often severe corrosion due to very aggressive components in the used fuels. High velocity oxy-fuel (HVOF) coatings offer excellent protection for boiler tubes against high temperature corrosion due to their high density and good adherence to the substrate material. Several thermal spray coatings with high chromium content were sprayed with HVOF technique. Their mechanical properties and high temperature corrosion resistance were tested and analyzed. The coating materials included NiCr, IN625, Ni-21Cr-10W-9Mo-4Cu, and iron-based partly amorphous alloy SHS9172 (Fe-25Cr-15W-12Nb-6Mo). High temperature corrosion testing was performed in NaCl-KCl-Na₂SO₄ salt with controlled H₂O atmosphere at 575 and 625 °C. The corrosion test results of the coatings were compared to corrosion resistance of tube materials (X20, Alloy 263 and Sanicro 25).

Keywords biofuel, coating characteristics, corrosion protection coating, CJS, high temperature corrosion, HVOF, molten salt, process optimization, waste to energy

1. Introduction

The need to decrease the carbon dioxide emissions in electricity and heat production has increased the use of biomass and waste together with coal (co-combustion), and also the number of biomass boilers and waste incinerators is increasing (Ref 1). In addition, the demand for higher efficiency of power and heat generation requires an increase in steam temperatures, which in turn raises material temperatures of boiler tubes. The utilization of difficult fuels such as biomass and solid recovered fuel (SRF), leads to very harsh conditions and may cause fouling, slagging, and severe high temperature corrosion of the metallic heat exchanger surfaces, e.g., active oxidation induced by chlorine, sulfidation, and molten salt attack (Ref 2-6). Corrosion problems can lead to material wastage, tube leakages, unplanned shutdowns of the boiler, and shortened lifetime of the boiler tubing; these are

very severe and expensive consequences of corrosion (Ref 7). Different thermal spray coatings can be applied to load carrying carbon steel or low alloyed steel tubes to increase the corrosion resistance and the lifetime of the tubes, e.g., superheaters. Thermal spray coatings offer a promising solution for corrosion protection as the material selection is very wide and the spraying can be optimized so that the coatings are well adhered and dense. Hence both the coating structure and the composition can be tailored for specific conditions.

Thermal spray coatings have a lamellar structure and the material composition can be selected quite freely. Main factors affect the formation of thermal spray coatings, such as selected method, raw material, gun, nozzle and fuels, and several process parameters, e.g., fuel ratio, spray distance, and powder feed rate. Thermal spray methods include flame, arc, plasma, high velocity oxy-fuel (HVOF), high velocity air-fuel (HVAF), detonation, and cold spraying. HVOF spraying is widely used for metallic materials due to its very high particle velocities which produce dense and well-adhered coatings. Different spray guns, nozzles, and fuels can be used to alter the temperature and velocity of the spray particles. Higher temperatures produce higher levels of molten particles and hence denser coating structure. When using higher particle velocities with lower particle temperatures, the particles maintain their original structure and composition better (e.g., nanostructure, volatile elements). The oxidation of metallic particles can be lower due to the shielding effect of the flame, the chemistry of the flame, and the lower particle temperature (Ref 8). The composition and the

Maria Oksa and Tommi Varis, VTT Technical Research Centre of Finland, Espoo, Finland; and Satu Tuurna, VTT Technical Research Centre of Finland, Tampere, Finland. Contact e-mail: maria.oksa@vtt.fi.

structure of the coatings should be tailored to endure general conditions as well as the harsh corrosion conditions to protect the low alloyed steel tubes. The coefficient of thermal expansion (CTE) of the coating should match with the substrate material in order to endure the thermal variations during the start-ups, shutdowns and the boiler process itself without cracking.

The operating conditions of different boilers (temperature, flue gas composition, fly ash, etc.) depend on fuels and process parameters and may vary inside the boiler. There are several high temperature corrosion mechanisms which can occur in power plant boilers utilizing chlorine-containing fuels. In the superheater area, corrosion derives from the reactions between fly ash, gaseous components, and cooler metal surface, on which a deposit is formed. The corrosion reactions are due to combustion gas containing HCl or deposited ash containing low melting point salts such as chlorides. Chlorine-induced active corrosion is very detrimental for steels, and the corrosion starts almost immediately after introduction of chlorine-containing contamination into the environment (Ref 9). Severe corrosion of the boiler tubes occurs especially by the molten phase (Ref 10, 11), and one of the very detrimental corrosion mechanisms in biomass and waste boilers is molten salt attack due to low melting temperature compounds, such as alkali metal chlorides (NaCl, KCl) and zinc or lead chlorides. (Ref 12, 13)

To overcome the high temperature chlorine-induced corrosion in power plant boilers, there are four different approaches: (1) maintain the steam temperature well below the temperature known for increased corrosion risk, (2) use additives to capture the alkali chlorides by sulfation before reaching the superheaters (Ref 14, 15), (3) develop and test new boiler tube materials, and (4) develop and test new coating materials. The high temperature corrosion of water walls is an important operational issue and a limiting factor in increasing the steam values, and consequently the electric efficiency (Ref 13). Especially with the waste fired power plants the first approach has to be used often due to very difficult fuels, which can cause severe corrosion even at temperature range 300-400 °C.

Several high temperature corrosion tests simulating biomass and waste incineration conditions on bulk materials and coatings, and the corrosion mechanisms involved have been reported in the literature (Ref 9-11, 16-23). However, optimizing and comparing structure of thermal spray coatings with two different HVOF methods, and testing of Ni-21Cr-10W-9Mo-4Cu (Diamalloy 4006) and SHS9172 coatings, and tube materials Alloy 263 and Sanicro 25 in molten alkali chloride salt has not been presented. The object was to prepare thermal spray coatings with two different HVOF methods, and compare their high temperature corrosion performance against severe corrosion attack induced by molten salt (Ref 24).

2. Experimental

Eight different coatings were manufactured by thermal spraying using an HVOF technique. Four different coating

materials were used (NiCr, IN625, Diamalloy 4006, and SHS9172) with two different HVOF spray guns: Carbide Jet Spray (CJS; by Thermico) and Diamond Jet Hybrid (DJ; by Sulzer Metco), which differ especially on particle temperature and velocity producing the coating due to different fuels (liquid-gas). The structure and mechanical properties (hardness and elastic modulus) of the coatings were analyzed. The high temperature corrosion resistance of the coatings against salt attack was tested in laboratory together with reference tube materials (X20, A263, and SAN25). The samples were analyzed by optical microscope and scanning electron microscope together with energy-dispersive X-ray analyzer (SEM-EDX). The detailed description of the materials, spray parameters, testing, and analyzing is presented in the following sections.

2.1 Coating Materials

Four coating materials were chosen for the testing: NiCr, IN625, Diamalloy 4006, and SHS9172. The powders and the manufacturers were Ni-980-1/1260F by Praxair (Praxair Surface Technologies, Indianapolis, IN, USA), Diamalloy 1005 (IN625) and 4006 by Sulzer (Sulzer Metco Europe GmbH, Hattersheim, Germany), and SHS 9172HV1 by Nanosteel (The Nanosteel Company, Providence, RI, USA). These alloys are designed for high temperature corrosion protection especially in harsh boiler conditions. Tables 1 and 2 present detailed information and compositions of the coating materials. The powders are not ideal for CJS spraying due to their coarse particle size.

2.2 Reference Tube Materials

Tube materials X20, A263, and SAN25 were used as reference materials in the high temperature corrosion testing. X20CrMoV121 (X20) is a ferritic stainless steel. In very demanding high temperature conditions the creep properties of ferritic or austenitic stainless steels are not adequate, and in those conditions nickel super alloys can be applied. Nimonic[®] alloy 263 (A263) is precipitation-hardenable and has high strength and corrosion resistance. Sanicro 25 by Sandvik (Sandviken, Sweden) (SAN25) is a recently developed iron-based alloy with excellent high temperature properties, designed for use in advanced pulverized coal fired steam boilers. The chemical composition of the reference materials is presented in Table 3.

2.3 Thermal Spray Coating Process

Thermal spray coatings were applied with HVOF technique using two different spray guns, Carbide Jet Spray (CJS) and Hybrid Diamond Jet (DJ Hybrid). Different fuels were used; kerosene and hydrogen for CJS, and propane (C₃H₈) for DJ. Applied spraying distance was 250 mm. Powder feed rate was 50 g/min for CJS and 40 g/min for DJ. Prior to spraying the test samples, different parameters were applied to optimize the structure of the coatings. Selected process parameters for each spraying are presented in Table 4. Temperature of the

Table 1 Powder information

Material	Powder code	Manufacturer	Particle size, μm	Manufactured	Morphology
NiCr	Ni-980-1/1260F	Praxair	-53 + 20	Gas atomized	Spheroidal
IN625	Diamalloy 1005	Sulzer Metco	-45 + 11	Gas atomized	Spheroidal
Diam4006	Diamalloy 4006	Sulzer Metco	-53 + 11	Water atomized	Irregular
SHS9172	SHS 9172HV1	Nanosteel	-53 + 15	Gas atomized	Spheroidal

Table 2 Chemical composition of powders according to manufacturer (wt.%)

Material	Ni	Fe	Cr	Mo	Nb	W	C	B	Mn	Si	Cu
NiCr	Bal.	1.1	>45	2.1	...
IN625	Bal.	2.5	21.5	9.0	3.7	0.1	0.2	...
Diam	Bal.	<1.0	20.5	9.0	...	10.0	0.75	0.75	4.0
SHS9172	...	Bal.	<25.0	<6.0	<12.0	<15.0	<4.0	<5.0	<3.0	<2.0	...

Table 3 Chemical composition of reference tube materials (wt.%)

	Fe	Ni	Cr	Mo	Co	W	Ti	V	Mn	Nb	Cu	C	Si	Al
X20	Bal.	0.3-0.8	10-12.5	0.8-1.2	0.25-0.35	<1	0.17-0.23	<0.5	...
A263	<0.7	Bal.	19-21	5.6-6.1	19-21	...	1.9-2.4	...	<0.6	...	<0.2	0.04-0.08	<0.4	<0.6
SAN25	Bal.	25	22.5	...	1.5	3.6	0.5	0.5	3	<0.1	0.2	...

Table 4 Process parameters for HVOF spraying (L/min). Spraying distance: 250 mm, and powder feed rate: 50 g/min CJS, 40 g/min for DJ

Coating	Spray method	H ₂	Keros.	O ₂	N ₂	Sweeps	Thickness, μm
NiCr	CJS, 140 mm	100	16	1000	6+6	21	220
IN625	CJS, 100 mm	100	16	1000	6+6	14	140
Diam	CJS, 100 mm	100	16	1000	6+6	14	280
SHS9172	CJS, 140 mm	100	16	850	6+6	10	250
Coating	Spray method	Propane	O ₂	Air	N ₂	Sweeps	Thickness, μm
NiCr	DJ, 2701	62.4	290	400	12.5	14	270
IN625	DJ, 2701	62.4	290	400	12.5	21	210
Diam	DJ, 2701	62.4	290	400	12.5	21	210
SHS9172	DJ, 2701	62.4	290	400	12.5	14	430

substrate material during spraying was measured with infrared thermometer and it varied between 180 and 230 °C. The spraying was performed on rotated X20 steel rings, with concurrent air cooling. CJS spray gun produces higher velocity and lower temperature compared to DJ, and hence produces very dense coatings with minor oxidation of the metallic coating material during the spraying (Ref 25). CJS is very well suited for spraying small particles with e.g., nanostructures, because the lower temperature enables the particle structure to be maintained in the coating. However, the thermal energy is not always high enough to give sufficient melting state to the coarse particles, which may cause lower cohesion between lamellas and detachment of the lamellas.

2.4 Testing Methods

After spraying, the coated rings were cut into sections of about $12 \times 20 \times 3$ mm, and one piece of each coating was prepared for metallurgical cross-section for optical microscopy analysis and mechanical testing, and one piece for high temperature corrosion testing.

Hardness (HV0.3) and elastic modulus (E_{IT}) were determined with an instrumented Zwick ZHU 0.2 hardness tester using the cross-sections of the coating samples. Elemental analysis of oxygen was performed by an inert gas fusion principle with a TC-436 LECO instrument. Separate coating samples were sprayed on standard porous disk substrates in parallel for measuring viscous gas

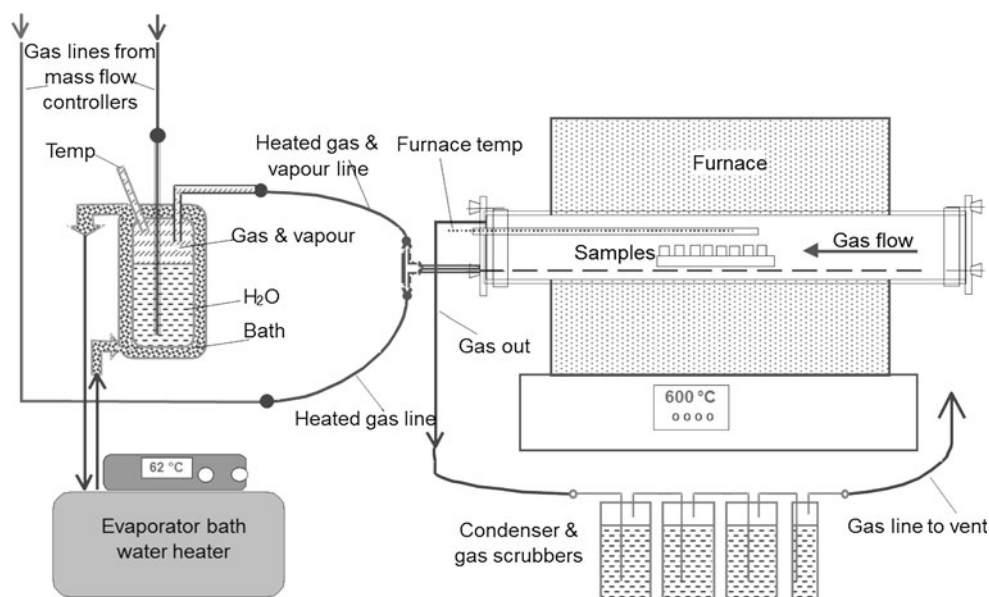


Fig. 1 Furnace layout of the high temperature corrosion testing

Table 5 Conditions used for the corrosion tests

Test	Temperature, °C	Salt	Gas	Duration, h
1	575	NaCl, Na ₂ SO ₄ , KCl	Synthetic air + 10% H ₂ O	168
2	625	NaCl, Na ₂ SO ₄ , KCl	Synthetic air + 10% H ₂ O	168

permeability coefficient with Coating Gas Permeability Tester (GPT-02) device by Kermetico, Inc. (Benicia, CA, USA). The test measures gas flow through a coating, which is directly correlated to the coating through porosity.

Two high temperature salt deposit corrosion tests were carried out in a high temperature corrosion test furnace with controlled conditions. The test layout is presented in Fig. 1. The deposit tests were performed to simulate the actual situation in boilers, where molten salt deposits may form on the tubes and cause severe corrosion. The tests were made in controlled atmosphere with synthetic air and 10% H₂O with salt deposit. The gas flow was controlled by mass flow controllers. The duration of each test was 168 h in total, with constant temperature of either 575 or 625 °C. The applied deposit was alkali chloride-alkali sulfate salt mixture of eutectic composition, which transforms in the molten state in 520-530 °C, 6.5 wt.% NaCl; 59 wt.% Na₂SO₄; and 34.5 wt.% KCl. The test conditions are presented in Table 5. The water soluble deposits were sprayed onto preheated (150-200 °C) samples following the TESTCORR recommended procedures (Ref 26). Deposit application was made on one side of the samples.

2.5 Characterization

After the corrosion tests, metallographic cross-sections were prepared by mounting the samples into resin, grinding and polishing with ethanol. Water was not used in

any part of the sample preparation to prevent the dissolution of water soluble compounds, such as chlorides. The characterization was performed visually, with an optical microscope, and a SEM-EDX.

3. Results and Discussion

3.1 Coating Characteristics

The mechanical properties of the coatings were tested before the corrosion exposure. The hardness of the coatings varied from 413 HV0.3, NiCr sprayed with CJS, to 1017 HV0.3 of SHS9172 coating sprayed with DJ. The SHS9172 coating contains fine carbides and borides, which explains much higher hardness values. The SHS9172 coating is therefore suitable also for erosion protection. The hardness values of the coatings were higher with DJ than with CJS. The elastic modulus of the coatings varied between 145 and 191 GPa. The highest values were achieved with CJS. The use of liquid fuels enables higher particle velocities compared to gas-fuelled system (Ref 27, 28), which has caused the higher elastic modulus for CJS sprayed coatings. The coating SHS9172 had the highest values with both spray methods. The mechanical properties hardness and elastic modulus of the coatings before the corrosion testing are presented in Fig. 2.

The oxygen content of the coatings was measured to compare the two HVOF processes and also to study the

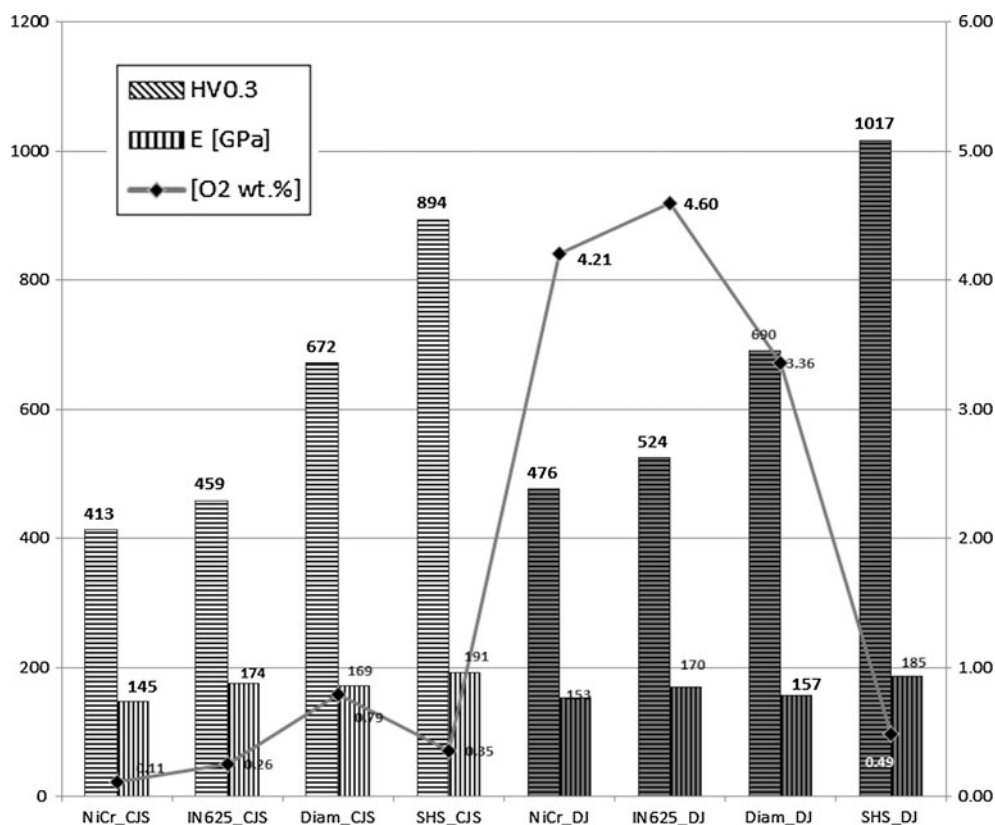


Fig. 2 Mechanical properties (left axis) and oxygen content (right axis) of the coatings. DJ Hybrid process produces higher hardness values than CJS process, whereas the elastic modulus is slightly higher when sprayed with CJS except with NiCr. With the CJS process less oxygen is formed into the coatings

effect of oxygen in the coatings on the corrosion properties. With the CJS spray gun less oxygen was captured by the coatings. The amount of oxygen varied between 0.11 and 0.79 wt.%. With the DJ system, the oxygen content was 0.49–4.60 wt.%. The oxygen content of the coatings is presented in Fig. 2. A previous study has shown (Ref 25) that the DJ Hybrid system produces a more oxidized metallic coating due to higher temperature and lower velocity of the spray particles compared to CJS, because it causes longer dwell time and hence reaction time with air during spraying (Ref 29). The powder is also fed into the combustion chamber with DJ, whereas with CJS it is fed into the nozzle with lower temperature. Both HVOF systems produced low oxide content for SHS9172 coating. Viscous gas permeability coefficients were measured for all CJS and two DJ sprayed coatings. The test measures N_2 gas flow through the coating. NiCr_DJ and Diam_DJ were gastight according to the measurement. The results are presented in Fig. 3.

The appearance of the coatings shows a clear difference between the CJS and DJ spraying. The melting state and oxidation of the coatings sprayed with DJ is higher than with CJS. The optical micrographs of the coating cross-sections are presented in Fig. 3. Because a sufficiently fine-grained powder was not used for NiCr_CJS, the melting of the powder particles was low, and individual splats can be seen in the coating, Fig. 3(a). Similar problems can be seen

for IN625_CJS, Fig. 3(b). To improve the quality of a CJS coating, the heating of the powder should be increased either with raising the temperature of the flame, or increasing the dwell time. This can be performed by decreasing the flow of oxygen, increasing the flow of kerosene, or using a longer gun barrel. Higher melting state and higher amount of oxygen can be distinguished from the micrographs by very flat splat structure and darker areas in the coatings NiCr_DJ, IN625_DJ, and Diam4006_DJ, Fig. 3(e)–(g). SHS9172 coating had also a higher melting state when sprayed with DJ compared to CJS, Fig. 3(d) and (h). However, coating SHS9172_DJ had few perpendicular cracks, which reached down into the substrate.

SHS9172_CJS coating did not show any cracking. This is due to higher particle velocity, which has induced compressive stresses into the coating. The differences in the coating structure, lower density (more porosity), and lamella shape (globular) have had a positive effect on preventing the cracking. Factors influencing the cracking are tensile residual stresses due to higher temperature and lower velocity of DJ spray (Ref 25), a mismatch of thermal expansion coefficient between the coating and substrate material (Ref 22), and shrinkage solidification due to rapid cooling from higher temperature when sprayed with DJ. This can be clarified and solved in future with spray optimization tools, which can measure particle velocity and temperature, detect formed stresses, and measure

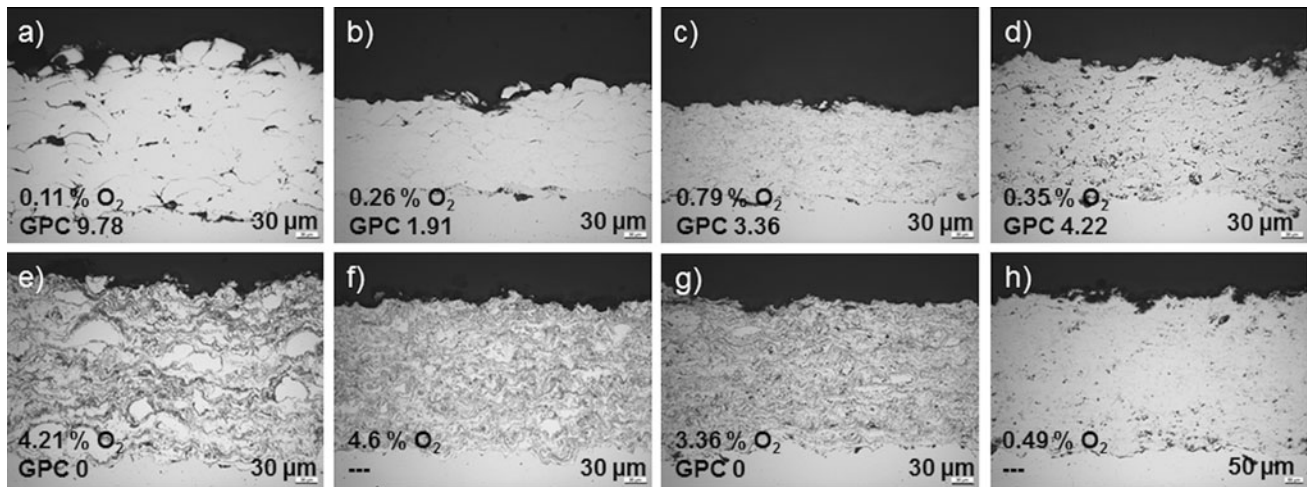


Fig. 3 Optical images of the coatings before the testing. (a) NiCr_CJS, (b) IN625_CJS, (c) Diam4006_CJS, (d) SHS9172_CJS, (e) NiCr_DJ, (f) IN625_DJ, (g) Diam4006_DJ, and (h) SHS9172_DJ. Oxygen content (wt.%), and viscous gas permeability coefficients (GPC) of the coatings (f and h not measured)

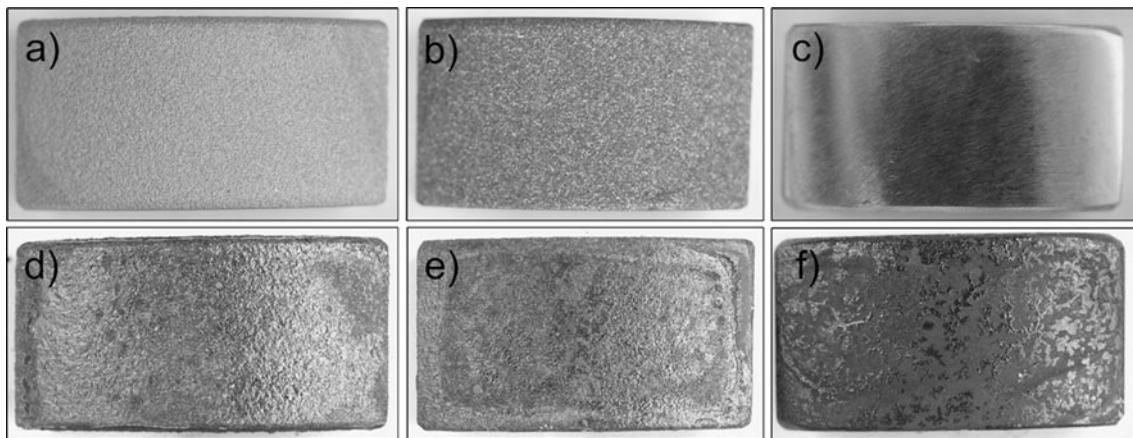


Fig. 4 Samples before the testing: (a) NiCr_CJS, (b) NiCr_DJ, (c) A263, and after the testing at 575 °C: (d) NiCr_CJS, (e) NiCr_DJ, and (f) A263. The NiCr coatings were covered with yellow-green deposit, whereas the A263 material had a darker deposit layer

CTE of the coating, and with a careful pre-heating and a controlled cooling of the coating sample.

The porosity of the coatings according to the appearance of the coatings and results from viscous gas permeability measurements were not as low as expected for CJS. There was interconnected porosity and low cohesion between the lamellas especially with NiCr_CJS coating, which was due to insufficient melting of a coarse powder. However, excellent results were achieved with NiCr_DJ and Diam4006_DJ, which could block penetration of N_2 gas flow through the coating. The higher melting state and flat lamellar structure of the DJ coatings was due to the higher heat input of the DJ spraying. The selection of powder has influence on the coating quality, and for CJS smaller particle size would be preferential, as the heat input in the system was not able to induce higher melting state for bigger particles (Ref 28).

3.2 High Temperature Corrosion Tests

Corrosion testing of the coatings and the reference tube materials was performed so that one side of the samples was covered with salt layer. The images of the upper sides of the samples before and after the corrosion testing at 575 °C are presented in Fig. 4. After the test at 575 °C, there was a yellow-green deposit layer on the NiCr coatings and on the Diam4006 coating sprayed with CJS. IN625, SHS9172, and Diam4006_DJ coatings were covered with dark red/partly yellow deposit layers. The coatings showed similar deposits as at higher temperature. NiCr, IN625 and Diam4006_DJ were covered with yellow-greenish deposit, and Diam4006_CJS and SHS9172_DJ had a dark reddish layer. Exception was SHS9172_CJS, which was covered mainly with a dark gray deposit layer. Maximum thickness of the oxide/corrosion layers was

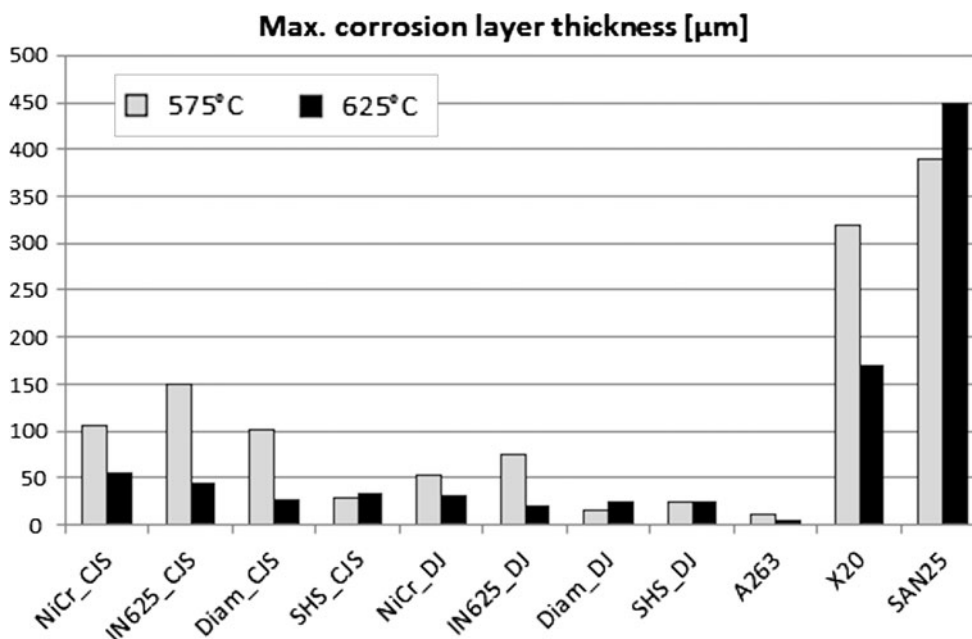


Fig. 5 Maximum thickness values of the oxide/corrosion layers formed during the tests (μm). Coatings performed better than X20 or SAN25, but nickel-based alloy A263 performed best. Due to its high price, coatings offer an attractive alternative for corrosion protection. Diam4006_DJ and SHS9172_CJS presented the best corrosion performance of the coatings

measured from the cross-sections. The values are presented in Fig. 5.

3.2.1 NiCr Coatings. NiCr coatings showed considerably better corrosion resistance than reference iron-based tube materials. The corrosion layer thickness was about 1/10 to 1/3 of the X20 or SAN25. NiCr_DJ coatings with higher density performed better. NiCr_CJS had suffered from the exposure especially at 575 °C and it failed due to its poor coating quality. The oxide layer consisted mainly of chromium oxide and contained a small amount of chlorine and sulfur. Chlorine had reacted with outer surface of the coating and it was detected also in the lamellar boundary near the coating surface (10 μm). Detachment of lamellas had taken place. SEM images of the cross-sections after the testing are presented in Fig. 6(a) and (d). The layer formed on NiCr_DJ was composed of chromium oxide together with potassium, sodium, and sulfur. The coating beneath the layer seemed dense. However, in the EDX analysis it was observed that chlorine had penetrated deeper into the coating (about 120 μm), and depletion of chromium from the coating was observed, Fig. 7. Difference in the structure and the corrosion behavior of NiCr coating with different spray methods can be seen in Fig. 6(a) and (d). NiCr_CJS had a broken oxide layer and severe detachment of lamellas had occurred.

A porous chromium oxide layer containing nickel and chlorine had built up on the NiCr coatings. The surface of the NiCr coating had a high content of nickel and was depleted of chromium. At 575 °C, there was also an outer mixed chromium oxide layer with potassium, sodium, sulfur, and chlorine on NiCr_DJ. The corrosion mechanism with NiCr coating has been dissolution of chromia caused by molten chlorine according to reaction (1)

(Ref 9), which explains the presence of potassium and sodium in the scale (Ref 11). The reaction of the melt with Cr_2O_3 has led to a depletion of chromium in the alloy and the nickel-rich spinels and nickel oxide may have formed.



3.2.2 IN625 Coatings. IN625 coatings showed similar corrosion resistance as NiCr coatings, and the corrosion layer thicknesses were 1/2 to 1/20 of the values of X20 and SAN25. However, IN625_CJS had a detached, thick corrosion layer, and some detachment of the outer lamellas had occurred. The oxide layer consisted mainly of chromium and iron oxide, with a very small amount of chlorine. IN625_DJ had an oxide layer, which was Cr-rich oxide near the coating and further Fe-rich. Small amount of chlorine was detected in the oxide layer, as well as at lamellar boundary near the surface. The effect of the test temperature on IN625_DJ is presented in Fig. 6(b) and (e). At lower temperature, the oxide layer was thicker and consisted mainly of iron oxide. At higher temperature, there was a thinner chromium oxide layer.

The coatings had an outer iron oxide rich layer, and near the coating surface there was a layer with chromium oxide. The layers contained chlorine. Also small amount of chlorine was detected at a lamellar boundary just below the outer surface of coating. The IN625 coating surface was rich in nickel and depleted of chromium. At higher temperature, only a chromium layer formed on the surface. DJ had produced better density for the IN625 coating, but at lower test temperature chlorine had penetrated into the coating. The corrosion mechanism on the CJS sprayed coating has probably been active oxidation, which has been enhanced by low thickness of the coating and

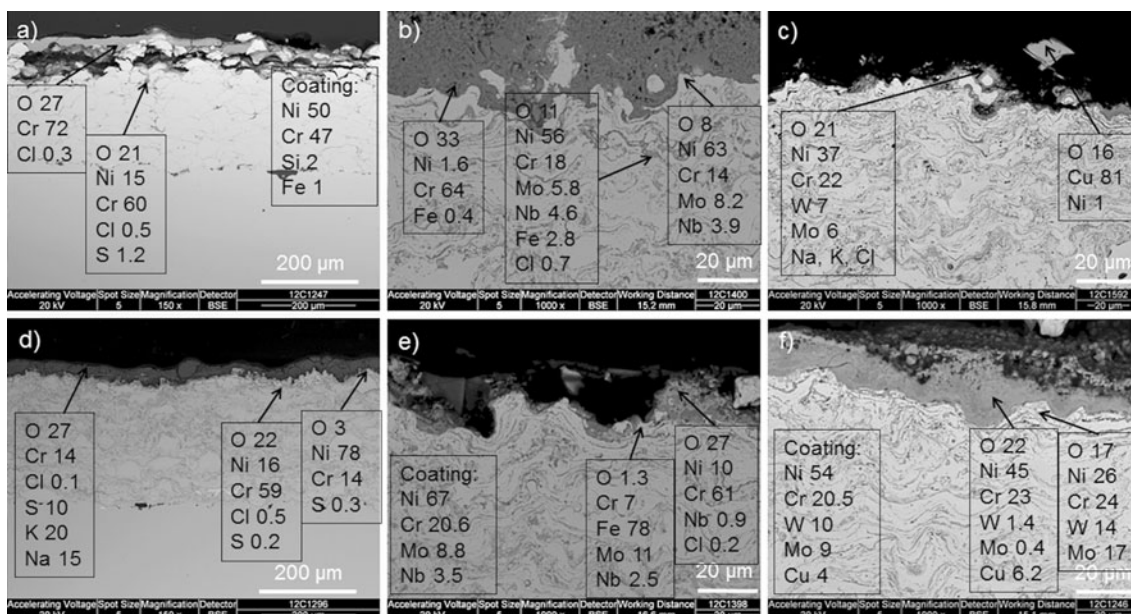


Fig. 6 SEM images (BSE—back-scattered electrons) after the testing: (a) NiCr_CJS (575 °C), (b) IN625_DJ (575 °C), (c) Diam4006_DJ (575 °C), (d) NiCr_DJ (575 °C), (e) IN625_DJ (625 °C), and (f) and Diam4006_DJ (625 °C). Main elements in the oxides or coating surfaces are presented in the figures. Penetration of corrosion through lamellar boundaries and detachment of outer lamellas due to corrosion reactions can be seen in the micrograph (a)

interconnected porosity. The lamellar boundaries have acted as easy path for chlorine penetration through the coating. Below the scale, chromium was selectively attacked by chlorine, which has been reported to increase the corrosion rate significantly above 520 °C (Ref 12). The outer surface of the coating contained only about 7 wt.% of chromium. Iron was detected in the coating (up to 6 %), which indicates formation of volatile iron chlorides at the coating/substrate interface (Ref 20). With high alloy steels, mainly FeCl_2 is formed due to its higher thermodynamic stability compared to NiCl_2 , CoCl_2 , CrCl_2 (Ref 9). At higher temperature the corrosion mechanism indicates the reaction of chromia with the melt.

3.2.3 DIAM4006 Coatings. The corrosion behavior of Diam4006 coatings differed strongly depending on the different spray system in similar way as with NiCr and IN625 coatings. Diam4006 presented excellent corrosion resistance compared to the reference materials X20 and SAN25. However, with CJS, the Diam4006 coating had experienced strong corrosion with an about 100 μm thick corrosion layer, which consisted mainly of iron, chromium, and oxygen, with small amounts of, e.g., chlorine, potassium, and sulfur. Interestingly, there were particles with high amount of copper and oxygen found above the oxide layer. Diam4006_DJ had endured the test well with only 15 μm thick oxide layer, with nickel, chromium, tungsten, and molybdenum. Chlorine was, however, observed in a lamellar boundary near the surface.

Figure 6(c) and (f) presents the effect of temperature for Diam4006_DJ coating. At lower temperature, a thin oxide containing nickel, chromium, molybdenum, and tungsten was formed. A detached copper oxide particle was detected on the surface. At higher temperature, a

slightly thicker oxide layer with nickel, chromium, copper, and niobium was formed on the coating. The outer surface of the coating was depleted of Ni and enriched with Mo and W. A SEM image and a point analysis of Diam4006_CJS oxide layer is presented in Fig. 8(a). Outermost there was a similar detached copper-rich oxide as with the Diam4006_DJ coating. The oxide layer had an iron-rich area further away the coating surface, and a chromium-rich area close to the coating, and the innermost oxide consisted of Ni, Cr, Fe, and chlorine.

The appearance of the Diam4006_CJS coating and EDX analysis support the assumption that the coating had experienced active oxidation. Diam4006_DJ performed better at lower temperature test, forming a thin oxide containing nickel, chromium, copper, and chlorine. At 625 °C both Diam4006 coatings had formed an oxide layer with nickel, chromium, and copper. Cu and Ni have much lower affinity for oxygen than do iron and chromium. Copper becomes concentrated at the scale/alloy interface as the more reactive elements become oxidized, and the alloy recedes. When copper, being the last element to oxidize, reaches the top of the scale, it is considered to oxidize to Cu^{2+} state (Ref 29). This can explain the presence of copper oxide at the outermost of the scale. Presence of copper compounds has been reported to increase corrosion rate significantly (the Deacon reaction) (Ref 30, 31). Therefore copper alloying can be detrimental in chlorine-containing atmospheres.

3.2.4 SHS9172 Coatings. Both SHS9172 coatings had endured in the test well against the corrosion attack compared to X20 and SAN25 with corrosion layer thicknesses of 1/20 to 1/5 of the values of the reference materials. The coatings were dense and had corrosion layers of

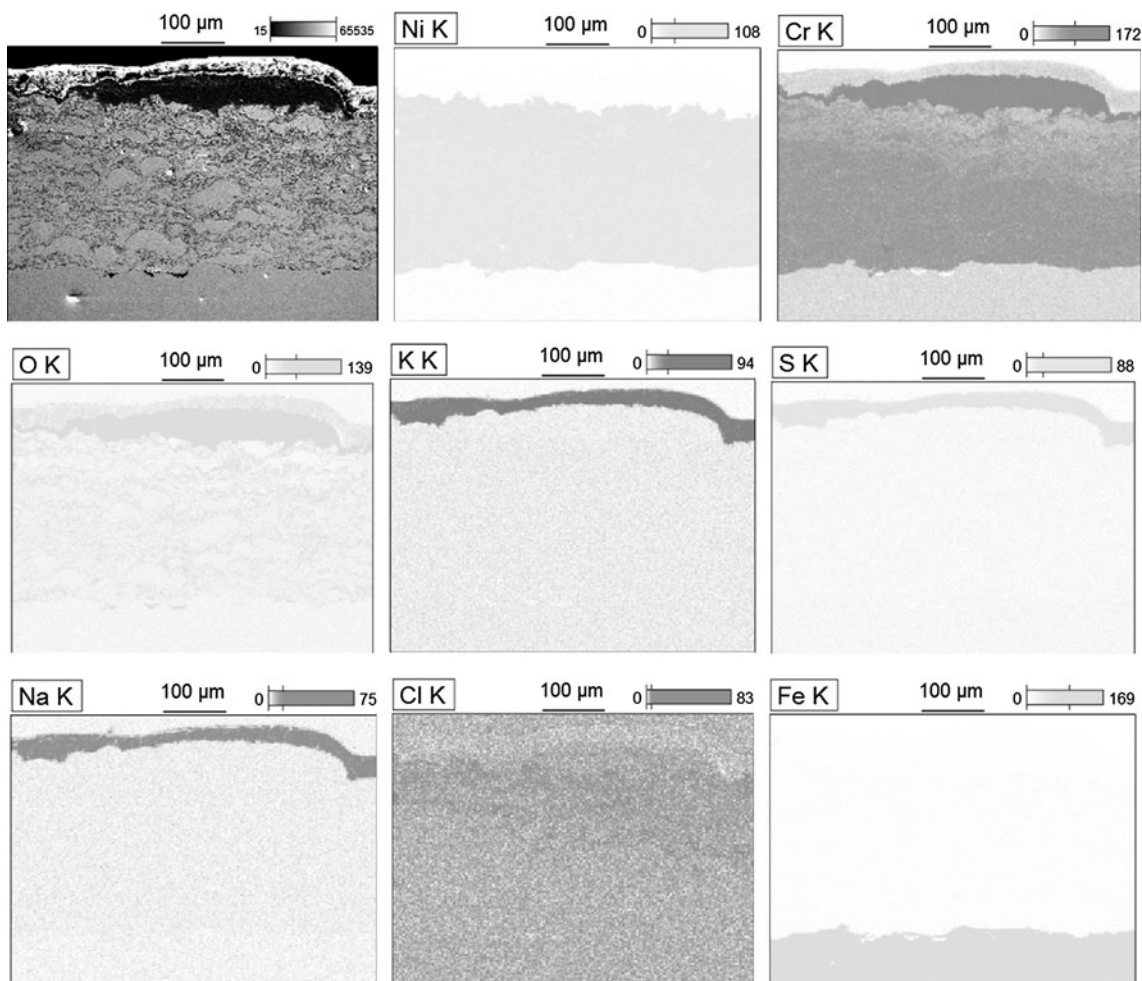


Fig. 7 EDX mapping of NiCr_DJ coating after the test at 575 °C. Chromium has diffused from the coating to form oxide in the surface. Chlorine has penetrated into the coating

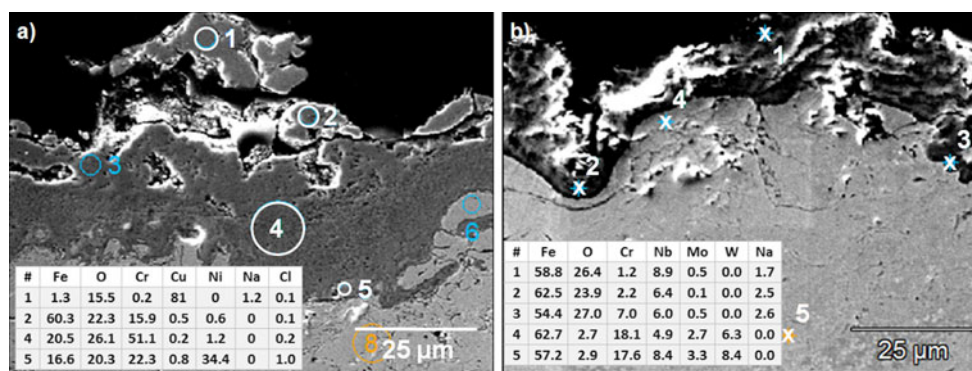


Fig. 8 SEM images of the cross-sections and EDX point analyses of (a) Diam4006_CJS (575 °C), and (b) SHS9172_DJ (575 °C) coating

about 25-30 μm and only slight detachment of the lamellas was found. The oxide layer consisted mainly of iron and chromium oxide with a small amount of sodium. The iron oxide on SHS9172_CJS was rich in niobium near the coating surface. Chlorine was detected only on lamellar

boundary of SHS9172_CJS (625 °C), not in the oxide layers. At lower temperature, a small amount of chlorine was present in the oxide and at the outer surface of the coating. The iron oxide layer on the SHS9172_DJ coating consisted of small amounts of Cr, Si, Mn, Mo, and Nb.

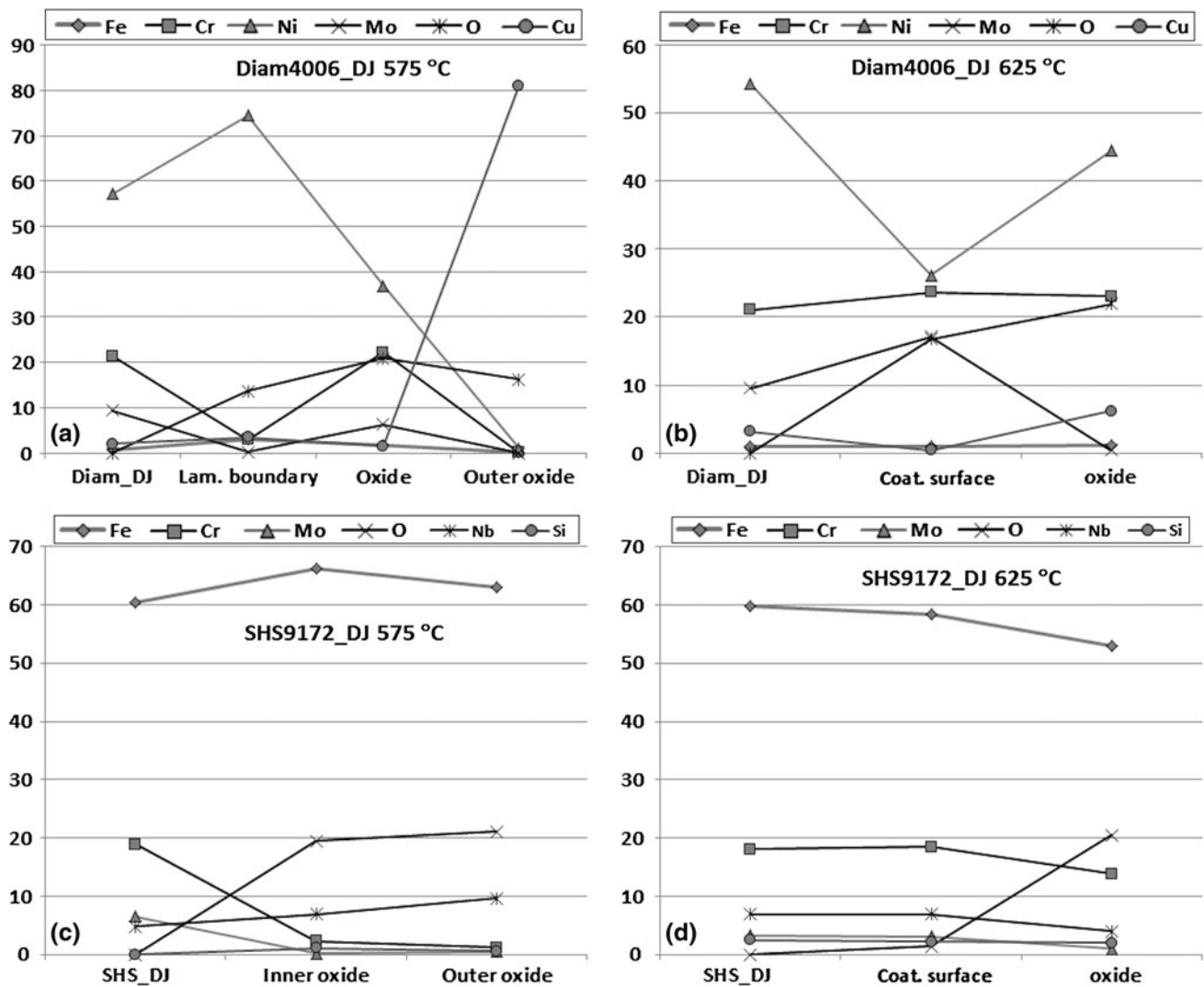


Fig. 9 Results of EDX analyses for Diam4006_DJ and SHS9172_DJ coatings: (a) DIAM4006_DJ at 575 °C, (b) DIAM4006_DJ at 625 °C, (c) SHS9172_DJ at 575 °C, (d) SHS9172_DJ at 625 °C. Main elements are presented (wt.%). Inner oxide presents the composition in the oxide layer nearest to the coating surface. The outer oxide is analyzed at the outer area of the oxide scale

SHS9172_DJ coating, which showed a very good corrosion resistance at both test temperatures, is presented in Fig. 8(b) together with an EDX analysis.

The formation of protective silicon and chromium oxides may have improved the corrosion resistance of SHS9172 coating (Ref 16). Also addition of molybdenum may have decreased the corrosion rate in the test conditions (Ref 19). The effect of the alloying elements and the partly amorphous structure on the excellent corrosion resistance needs further investigation. Main elements on EDX results of Diam4006_DJ and SHS9172_DJ, which showed the highest corrosion resistance, are presented in Fig. 9(a)-(d). However, the coating with DJ had few vertical cracks down to the substrate material, and therefore does not protect the substrate material. Cracking of the SHS9172_DJ coating should be prevented by better process optimization, which includes variation of process parameters, use of

diagnostic tools, sufficient control on pre-heating and cooling of the coating, and possibly use of a bond coat to prevent mismatch in CTE between the coating and the substrate material.

3.2.5 X20 Tube Material. The corrosion resistance of ferritic steel X20 was not expected to be sufficient in the test conditions due to low amount of alloying elements (Ref 3, 5). The material experienced severe corrosion at both test temperatures. The corrosion layers were porous and detached with multilayer oxides, mainly consisting of Fe_2O_3 , with some sulfur, chlorine, and potassium, Fig. 10(a) and (b). At the metal surface of X20 there was a Ni-rich oxide present after both tests. Fe-Cr steels have high corrosion rates in conditions containing chlorine, and especially molten chlorides due to fluxing (dissolution) and destruction of the oxide (Ref 11). The formation of a protective oxide layer is not possible in the conditions and the corrosion rate is increased.

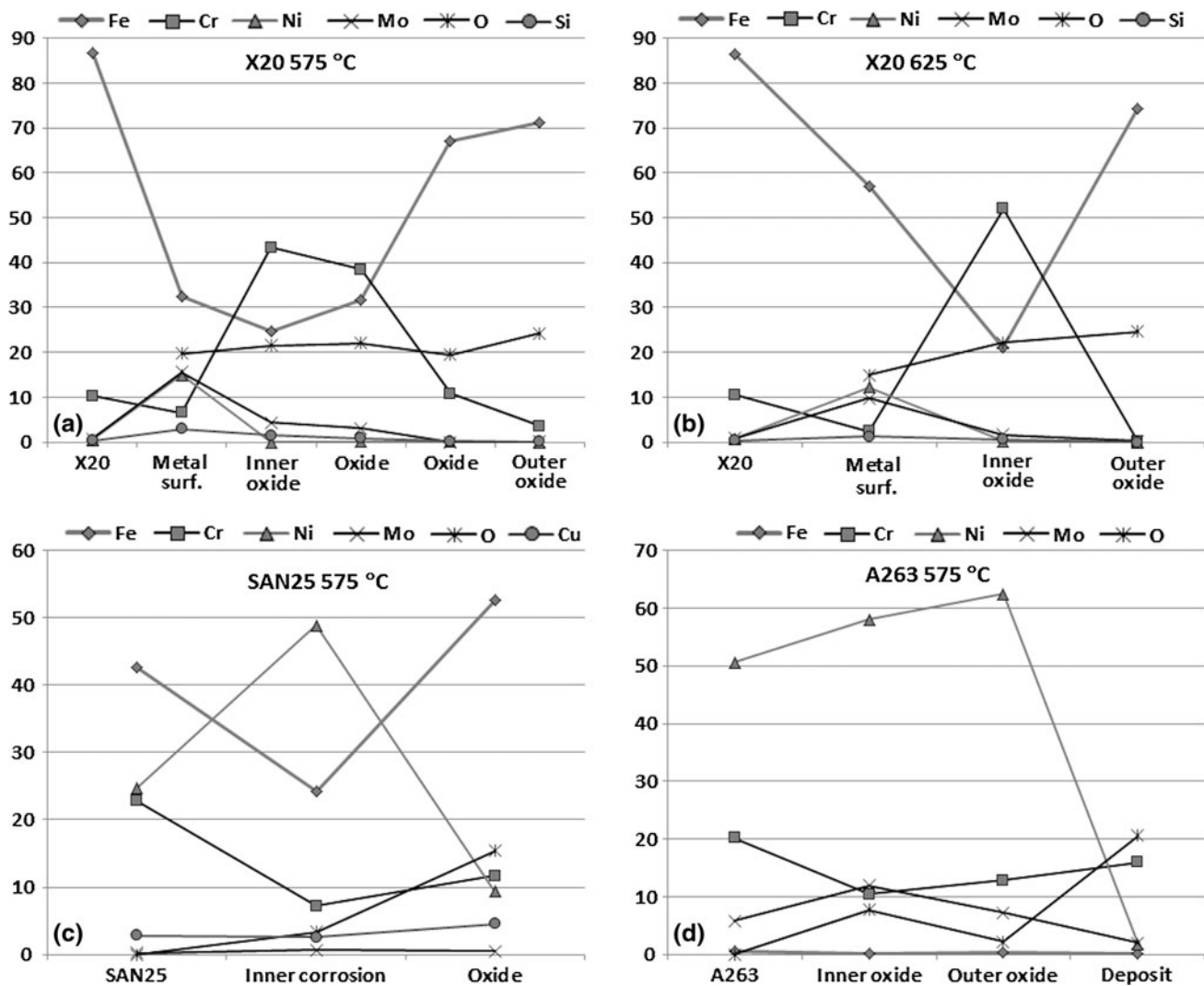


Fig. 10 Results of EDX analyses for materials X20, A263, and SAN25: (a) X20 at 575 °C, (b) X20 at 625 °C, (c) A263 at 575 °C, (d) SAN25 at 575 °C. Main elements are presented

3.2.6 SAN25 Tube Material. Austenitic alloy SAN25 had suffered from disastrous corrosion during the tests. The oxides were thick, detached, and contained chlorine. Outermost, there was iron oxide and a thin Cu-Na-O layer above it, Fig. 10(c). Next there was a chromium oxide layer. The innermost layer consisted of Ni, Cu, O, and small amounts of sodium, sulfur, chlorine, and potassium. Corrosion had progressed through grain boundaries under the oxide layer about 100 μm deep. The grain boundary attack was induced by chlorine, and the corrosion area was depleted of chromium and contained chlorine. SEM images with EDX mapping of SAN25 are presented in Fig. 11. SAN25 contains copper as well as the Diam4006 coating material. Copper was found on in the outer layer of the formed oxides with both materials. With SAN25, copper was found in the Ni-rich inner oxide and as a thin outermost Cu-Na-O layer.

The corrosion of SAN25 may have followed mechanism described by Spiegel (Ref 11). The stability of chlorides and sulfates in deposits, and their effect on

corrosion mechanisms, are strongly dependent on partial pressure of oxygen and water vapor, HCl/SO₂ ratio, temperature of the gas phase and composition of the deposits on the tubes. At first, a chromium-rich oxide layer is formed on the alloy surface. After deposition of fly ash and reaction with melt in the deposits, this layer is destroyed. The reaction of the melt with an initially formed chromia scale may occur according to (Ref 11):



Reaction of the melt with Cr₂O₃ leads to a depletion of chromium in the alloy and the nickel-rich spinels and nickel oxide can form. Because NiO scale is very porous, flue gas and volatile salts can diffuse to the scale/melt interface and condense as solid or molten phases, and corrosive attack can continue.

SAN25 is designed for ultra-supercritical coal fired boilers, where this kind of atmosphere causing

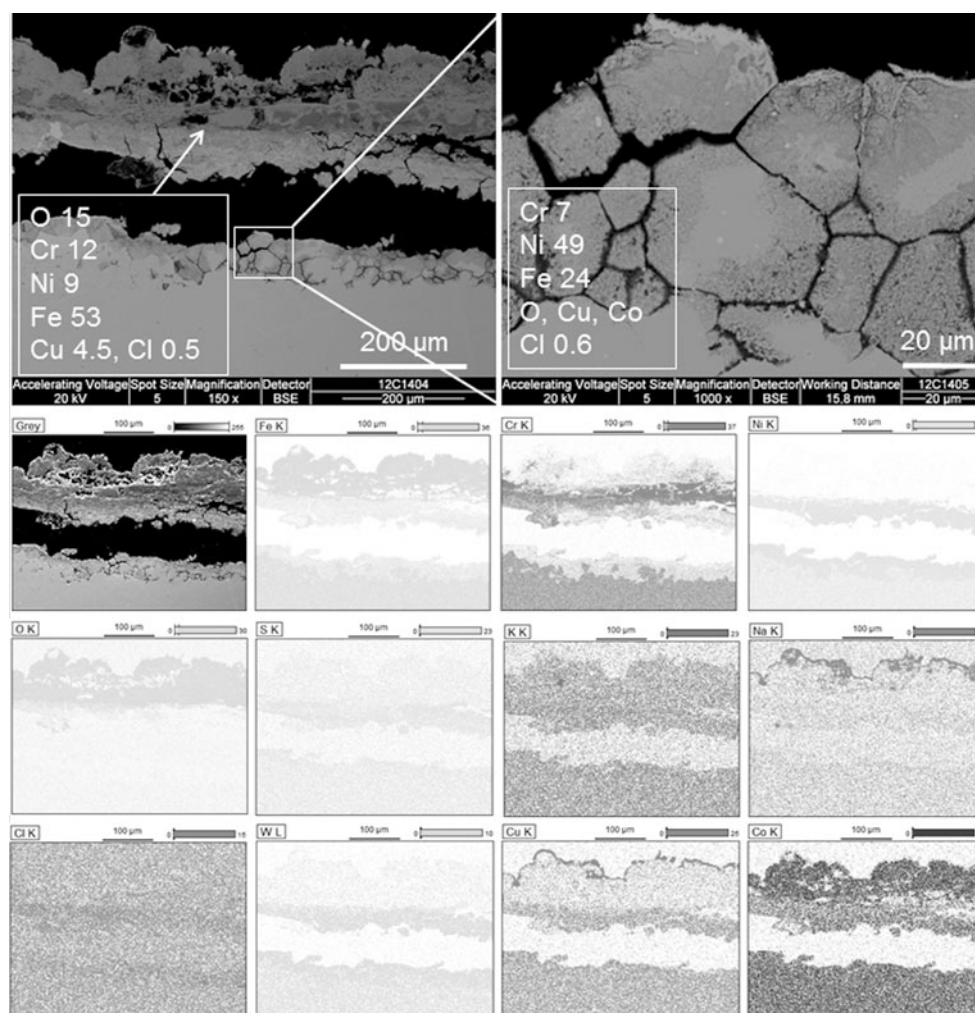


Fig. 11 SEM images (BSE) of material SAN25 after the test at 575 °C, and EDX mapping of the corrosion layer elements. Chlorine was detected in the corrosion layer and on the metal surface with intergranular corrosion

catastrophic corrosion is not likely to occur (Ref 29). However, SAN25 cannot be recommended to severe conditions with any risk of molten salt attack by chlorine.

3.2.7 A263 Tube Material. Ni alloys have been reported to have much better corrosion resistance compared to Cr steels (Ref 16, 18). The corrosion resistance of nickel alloy A263 was proved excellent in the tests. The oxide layer formed at 575 °C consisted of nickel, chromium, cobalt, titanium, molybdenum, and small amounts of sulfur, potassium, and chlorine, Fig. 10(d). The precipitation hardened Ni-alloy with sufficient creep and fatigue strength could be used at high temperature envisaged for ultra-supercritical pulverized coal fired boilers. However, the high price and expensive machining of the material are restricting its use.

3.2.8 Corrosion Performance. The coatings offered sufficient protection against molten salt attack in most cases. Ni-based alloys showed significantly better corrosion resistance compared to the Fe-based reference tube materials X20 and SAN25. Somewhat surprising was the excellent performance of the Fe-based SHS9172 coating.

Despite the good results in the short-term laboratory tests, a longer exposure in such a severe corrosion condition might cause penetration of corrosive elements, especially chlorine, to substrate and induce active corrosion at the interface. The long-term resistance of the coatings will be tested in a real biomass boiler exposure as controlled probe measurements.

Most important factors to the corrosion resistance against molten salt corrosion proved to be suitable alloying and an optimized dense coating structure. The corrosion protection of any alloy against salt melt attack depends on the chemical stability on both the kinds of metal and their compounds such as oxides and chlorides (Ref 18). Even though chromia has high solubility in NaCl-KCl melt (Ref 10), a sufficient amount of chromium (>18 wt.%) to form a protective chromium oxide on the surface was needed for better corrosion resistance based on the test results. Advantageous alloying elements in Diam4006 and SHS9172 against molten chloride salt corrosion were both molybdenum and niobium. The free energy of $\text{MoCl}_2/\text{NbCl}_2$ formation is considerably less



negative than for FeCl_2 and CrCl_2 (Ref 14, 15). Both coatings contained also a high amount of tungsten, but it is mainly to give high hardness (as carbides and borides). Silicon and aluminum have been observed to increase high temperature corrosion resistance in Fe-Cr and Ni-Al alloys (Ref 14), and they were found at oxides of well endured SHS9172. It was observed that lamellar boundaries are critical for corrosion performance, because they act as corrosion paths, for e.g., chlorine, potassium, and sulfur. Effect of oxygen in lamellar boundaries has been reported to be detrimental (Ref 20), and with the coating SHS9172 this applied. However, the structure of the other coatings with low oxygen was not sufficient to improve corrosion protection due to poor cohesion of lamellas.

The effect of the test temperatures was contradictory. In some cases, the lower 575 °C temperature was very detrimental. However, similar results in the temperature range 500-650 °C under alkali salt deposits have been reported (Ref 19, 21, 32), but no clear explanation to the phenomenon has been presented. Paul (Ref 21) suggested that the reason for better corrosion resistance at higher temperature was due to the change in predominant corrosion mechanism from molten salt corrosion to gaseous corrosion. Most probably the reason derives from sulfate-chloride chemistry and the ability of the metal or alloying elements to form a protective oxide in the prevailing conditions (Ref 9). It is assumed that the 50 °C increase of temperature may have enhanced the vaporization of chlorine, and the gas flow during the test could have decreased the amount of chlorine in the corrosion process. This was thermodynamically calculated with FactSage 6.2. According to calculation, the melting point of the salt mixture is 517 °C. The amount of vaporizing chlorine (and potassium) increases, even though the amount is very small. The kinetics of the process are difficult to estimate, because mass transfer constraints the vaporization. Another explanation may be higher diffusion rate of chromium or other protective component to form a more protective scale on the alloy, which could have retarded the corrosion process. This is supported by the higher amount of chromium in the oxide layers at 625 °C as compared to lower temperature.

4. Conclusions

Several thermal spray coatings were manufactured and tested against molten salt attack. The effect of two HVOF spray processes on coating characteristics and high temperature corrosion properties was studied. Four different coatings suitable for boiler applications were selected to the tests: nickel-based alloys with high chromium content NiCr, IN625, and Diam4006, and iron-based SHS9172. Coatings were sprayed with two HVOF techniques, CJS and DJ Hybrid. The mechanical properties of the coatings were analyzed and corrosion protection properties were tested with high temperature molten salt corrosion test at two temperatures (575 and 625 °C) for 168 h. The salt was composed of NaCl, KCl, and Na_2SO_4 . The conclusions are following:

- SHS9172 coating had high hardness and elastic modulus with both HVOF spraying. DJ produced higher hardness and CJS higher elastic modulus: HV0.3 894 (CJS) and 1017 (DJ); E_{IT} : 191 GPa (CJS) and 185 GPa (DJ).
- A higher melting state was produced with DJ Hybrid method, especially on NiCr, IN625, and Diam4006 coatings. This produced higher amount of oxygen into the coating, as well.
- Diamalloy 4006 coating sprayed with DJ and SHS9172 coating sprayed with CJS had the best high temperature corrosion properties against molten salt attack.
- SHS9172 coating (DJ) endured corrosion tests well, but vertical cracking should be prevented with sufficient coating optimization.
- NiCr (DJ) and IN625 (CJS, DJ) protected the substrate material, but formed thick corrosion layers especially at the 575 °C test.
- With NiCr, IN625, and Diam4006 high melting state produced better corrosion protection.

Based on the corrosion test results, the optimization of the coating structure besides selection of suitable chemical composition is critical. The spray technique and spray parameters have strong influence on, e.g., porosity, lamellar cohesion, melting state, oxidation, and adherence of the coating, and thus to corrosion protection properties. Dense HVOF coatings can offer good protection to the low alloy boiler tube materials even in harsh conditions, where molten salts may be present, and hence increase the lifetime of boiler tubes. Low porosity and good lamellar cohesion is very important with thermal spray coatings, as the lamellar boundaries act as corrosion paths and detachment of the lamellas may be high in harsh corrosion conditions. Therefore detailed optimization of the coating structure with suitable chemical composition should be performed carefully.

Acknowledgments

Mr. Mika Jokipii and Mr. Jarkko Metsäjoki are greatly acknowledged for their expertise. The authors would like to acknowledge the financial support of FP7 project NextGenPower—Meeting the Materials and Manufacturing Challenge for Ultra High Efficiency PF Power Plants with CCS, and all the partners involved.

References

1. L. Baxter, Biomass-Coal Co-Combustion: Opportunity for Affordable Renewable Energy, *Fuel*, 2005, **84**, p 1295-1302
2. H.P. Nielsen, F.J. Frandsen, K. Dam-Johansen, and L.L. Baxter, The Implications of Chlorine-Associated Corrosion on the Operation of Biomass-Fired Boilers, *Prog. Energy Combust. Sci.*, 2000, **26**, p 283-298
3. F.J. Frandsen, Utilizing Biomass and Waste for Power Production—A Decade of Contributing to the Understanding, Inter-

- pretation and Analysis of Deposits and Corrosion Products, *Fuel*, 2005, **84**, p 1277-1294
4. K. Persson, M. Broström, J. Carlsson, A. Nordin, and R. Backman, High Temperature Corrosion in a 65 MW Waste to Energy Plant, *Fuel Process. Technol.*, 2007, **88**, p 1178-1182
 5. M. Montgomery, T. Vilhelmsen, and S.A. Jensen, Potential High Temperature Corrosion Problems Due to Co-Firing of Biomass and Fossil Fuels, *Mater. Corros.*, 2008, **59**(10), p 783-793
 6. N. Otsuka, Chemistry and Melting Characteristics of Fireside Deposits Taken From Boiler Tubes in Waste Incinerators, *Corros. Sci.*, 2011, **53**, p 2269-2276
 7. M.J. Schofield, Corrosion, *Plant Engineer's Reference Book*, 2nd ed., D.A. Snow, Ed., Elsevier, Amsterdam, 2002, 9 p
 8. A. Valarezo, W.B. Choi, W. Chi, A. Gouldstone, and S. Sampath, Process Control and Characterization of NiCr Coatings by HVOF-DJ2700 System: A Process Map Approach, *J. Therm. Spray Technol.*, 2010, **19**(5), p 852-865
 9. H.J. Grabke, E. Reese, and M. Spiegel, The Effect of Chlorides, Hydrogen Chloride and Sulphur Dioxide in the Oxidation of Steels Below Deposits, *Corros. Sci.*, 1995, **37**(7), p 1023-1043
 10. T. Ishitsuka and K. Nose, Stability of Protective Oxide Films in Waste Incineration Environment-Solubility Measurements of Oxides in Molten Chlorides, *Corros. Sci.*, 2002, **44**(2), p 247-263
 11. M. Spiegel, Salt Melt Induced Corrosion of Metallic Materials in Waste Incineration Plants, *Mater. Corros.*, 1999, **50**, p 373-393
 12. H.P. Michelsen, F. Frandsen, K. Dam-Johansen, and O.H. Larsen, Deposition and High Temperature Corrosion in a 10 MW Straw Fired Boiler, *Fuel Process. Technol.*, 1998, **54**, p 95-108
 13. P. Vainikka, D. Bankiewicz, A. Frantsi, J. Silvennoinen, J. Hannula, P. Yrjas, and M. Hupa, High Temperature Corrosion of Boiler Waterwalls Induced by Chlorides and Bromides. Part 1: Occurrence of the Corrosive Ash Forming Elements in a Fluidised Bed Boiler Co-Firing Solid Recovered Fuel, *Fuel*, 2011, **90**, p 2055-2063
 14. P. Viklund, R. Pettersson, A. Hjörnhede, P. Henderson, and P. Sjövall, Effect of Sulphur Containing Additive on Initial Corrosion of Superheater Tubes in Waste Fired Boiler, *Corros. Eng. Sci. Technol.*, 2009, **44**(3), p 234-240
 15. M. Aho, P. Yrjas, R. Taipale, M. Hupa, and J. Silvennoinen, Reduction of Superheater Corrosion by Co-Firing Risky Biomass with Sewage Sludge, *Fuel*, 2010, **89**, p 2376-2386
 16. H.J. Grabke, M. Spiegel, and A. Zahs, Role of Alloying Elements and Carbides in the Chlorine-Induced Corrosion of Steels and Alloys, *Mater. Res.*, 2004, **7**(1), p 89-95
 17. Y. Kawahara, High Temperature Corrosion Mechanisms and Effect of Alloying Elements for Materials Used in Waste Incineration Environment, *Corros. Sci.*, 2002, **44**, p 223-245
 18. Y.S. Li, M. Spiegel, and S. Shimada, Corrosion Behaviour of Various Model Alloys With NaCl-KCl Coating, *Mater. Chem. Phys.*, 2005, **93**, p 217-223
 19. B.-J. Skrifvars, R. Backman, M. Hupa, K. Salmenoja, and E. Vakkilainen, Corrosion of Superheater Steel Materials under Alkali Salt Deposits Part 1: The Effect of Salt Deposit Composition and Temperature, *Corros. Sci.*, 2008, **50**, p 1274-1282
 20. M.A. Uusitalo, P.M.J. Vuoristo, and T.A. Mäntylä, High Temperature Corrosion of Coatings and Boiler Steels below Chlorine-Containing Salt Deposits, *Corros. Sci.*, 2004, **46**, p 1311-1331
 21. S. Paul and M.D.F. Harvey, Corrosion Testing of Ni Alloy HVOF Coatings in High Temperature Environments for Biomass Applications, *J. Therm. Spray Technol.*, 2013, **22**, p 316-327
 22. S.S. Chatha, H.S. Sidhu, and B.S. Sidhu, High Temperature Hot Corrosion Behaviour of NiCr and Cr₃C₂-NiCr Coatings on T91 Boiler Steel in an Aggressive Environment at 750 °C, *Surf. Coat. Technol.*, 2012, **206**(19-20), p 3839-3850
 23. T.S. Sidhu, S. Prakash, and R.D. Agrawal, Hot Corrosion Performance of a NiCr Coated Ni-Based Alloy, *Scr. Mater.*, 2006, **55**, p 179-182
 24. M. Oksa, S. Tuurna, and T. Varis, High Temperature Corrosion Resistance of HVOF Coatings in a NaCl-KCl-Na₂SO₄ Salt, *Proceedings of EUROCORR 2012*, September 9-13 (Stockholm, Sweden), European Federation of Corrosion, 2012, 12 p
 25. M. Oksa, T. Varis, T. Suhonen, and M. Jokipii, Optimizing NiCr Thermal Spray Coating with Process Map Methodology for High Temperature Power Plant Boiler Application, *Proceedings of International Thermal Spray Conference*, May 21-24 (Houston, Texas, USA), ASM International, 2012, 6 p
 26. A.B. Tomkings, J.R. Nicholls, D.G. Robertson, EC Report, EUR 19479 EN, Discontinuous Corrosion Testing in High Temperature Gaseous Atmospheres (TESTCORR), London, Directorate-General for Research, 2001
 27. S. Kamnis and S. Gu, 3-D Modelling of Kerosene-Fuelled HVOF Thermal Spray Gun, *Chem. Eng. Sci.*, 2006, **61**, p 5427-5439
 28. D. Zhang, S.J. Harris, and D.G. McCartney, Microstructure Formation and Corrosion Behaviour in HVOF-Sprayed Inconel 625 Coatings, *Mater. Sci. Eng. A*, 2003, **344**, p 45-56
 29. L. Intiso, L.-G. Johansson, S. Canovic, S. Bellini, J.-E. Svensson, and M. Halvarsson, Oxidation Behaviour of Sanicro 25 (42Fe22Cr25NiWCuNbN) in O₂/H₂O Mixture at 600 °C, *Oxid. Met.*, 2012, **77**, p 209-235
 30. K. Nakagawa and Y. Matsunaga, The Effect of Chemical Composition of Ash Deposit on the Corrosion of Boiler Tubes in Waste Incinerators, *Mater. Sci. Forum*, 1997, **251-254**, p 535-542
 31. M.C. Galetz, J.T. Bauer, M. Schutze, M. Noguchi, C. Takatoh, and H. Cho, The Influence of Copper in Ash Deposits on the Corrosion of Boiler Tube Alloys for Waste-to-Energy Plants, *Mater. Corros.*, 2012, **63**, p 1-8
 32. S. Enestam, D. Bankiewicz, J. Tuiremo, K. Mäkelä, and M. Hupa, Are NaCl and KCl Equally Corrosive on Superheater Materials of Steam Boilers?, *Fuel*, 2013, **104**, p 294-306